Surface & Coatings Technology 349 (2018) 773–782

Contents lists available at ScienceDirect

Surface & Coatings Technology

journal homepage: www.elsevier.com/locate/surfcoat

Design challenges in electrodepositing metal-anionic clay nanocomposites: Synthesis, characterization, and corrosion resistance of nickel-LDH nanocomposite coatings

Ryan E. Daugherty, Madeline M. Zumbach, Stephen F. Sanders, Teresa D. Golden*

1155 Union Circle #305070, Department of Chemistry, University of North Texas, Denton, TX 76203, USA

ARTICLE INFO

Keywords:
Layered double hydroxide
Nickel
Electrodeposition
Nanocomposite
Corrosion

ABSTRACT

A method was developed to electrochemically synthesize metal-anionic clay nanocomposite coatings. The coatings consist of Zn-Al layered double hydroxide (LDH) nanoplatelets incorporated into a nickel matrix (Ni-LDH), and were evaluated for their corrosion resistance versus pure nickel coatings on steel substrates. The LDH nanoplatelets incorporated into the nickel coatings were synthesized from zinc and aluminum nitrate salts using a refluxing coprecipitation method. These nitrate platelets were intercalated with sodium dodecylsulfate, increasing the gallery spacing from 9.06 Å to 37.6 Å, followed by refluxing in butanol to delaminate the LDH crystal sheets, giving a 1.5 g/L loading of LDH in the continuous phase. The average platelet size was found to be 631 ± 43 nm. Aliquots of the delaminated LDH colloid were added to a modified nickel bath for electrodeposition. Challenges for electrodepositing these metal anionic clay nanocomposites from an aqueous bath are reviewed and discussed. EDS analysis confirms the presence of the nanoplatelets in the metal coating. The resulting nanocomposite films have a preferred (220) orientation and crystallite sizes ranging from 25 to 60 nm as measured by XRD. Corrosion resistance of the coatings was also improved over the pure nickel coatings and measured in 3.5% NaCl with potentiodynamic polarization and electrochemical impedance spectroscopy. Suggestions for future design and improved properties are discussed for these types of nanocomposite coatings.

1. Introduction

A substantial amount of research has focused on metal matrix composite coatings for improved physical properties and corrosion resistance [1–4]. Inclusion of ceramic nanoparticles into a metal matrix can increase hardness, improve thermal stability, and provide better tribological properties [5–7]. Many ceramic materials such as Al_2O_3, TiO_2, CeO_2, and ZrO_2 have been successfully incorporated within metal matrices and shown to improve the mechanical properties of the electrodeposited coatings [8–11]. Additionally, previous work by our research group has shown successful incorporation of exfoliated montmorillonite (a cationic clay) nanoparticle platelets into nickel, Ni-Mo, and Cu-Ni coatings. These coatings had smaller crystallite size [12–14], and improved corrosion resistance when exposed to sodium chloride solutions, compared to the pure metal coatings.

Layered double hydroxides (LDHs) are a class of anionic clays with a wide variety of available elemental compositions, which make them an interesting candidate for incorporation into metal and alloy coatings as a means to improve corrosion properties. The crystallite layers consist of a combination of divalent and trivalent metal hydroxides in a sheet-like lattice framework with the general formula $[M(II)_{(1-x)}M'(III)_x(OH)_2]^{x+}A^{n-}_{x/n}\cdot mH_2O$, where M and M′ are a metal species, A is a charge balancing anion in the interlayer, n is the valence charge of the anion, and m is the empirical molar coefficient of complexed water. Trivalent species substitution causes the LDH lattice to exhibit a strong net positive charge due to a forced octahedral geometry. Accompanying anion species each electrostatically bind to two of these sheets to form large, net-neutral layered structures. The elemental composition, size, and anionic exchange capacity are variable and can be controlled through the synthetic process. There are 56 known divalent-trivalent combinations, most of which are capable of exhibiting multiple M(II):M(III) ratios [15]. The wide range of possible combinations is what makes combining LDH nanoparticles into metal coatings interesting, possibly giving unique and tunable properties. These anionic clays have already proved to be successful materials for corrosion resistance as pure coatings or as additives within polymer coatings [16–20]. However, incorporation into a metal matrix has not been explored and could lead to coatings with beneficial properties. A good metal candidate to combine with LDH nanoplatelets is nickel, since it is easy to electrodeposit and itself offers beneficial corrosion

* Corresponding author.
E-mail address: tgolden@unt.edu (T.D. Golden).

https://doi.org/10.1016/j.surfcoat.2018.05.026
Received 15 November 2017; Received in revised form 10 May 2018; Accepted 11 May 2018
Available online 12 May 2018
0257-8972/ © 2018 Elsevier B.V. All rights reserved.

protection [21]. Nickel coatings provide toughness and good general corrosion resistance but are susceptible to pitting and microbial induced corrosion, thus necessitating a need for alloying or inclusion of additives to improve their service life [22,23]. However, there are several obstacles to overcome in producing these types of metal-LDH nanocomposite coatings when using electrodeposition.

LDH delamination, to obtain individual nanoplatelets is difficult in water and has only been reported under certain circumstances. Thus it is not a good option for direct electrosynthesis of metal-LDH composite coatings [24,25]. Studies have shown that it is difficult to delaminate LDH compared to other silicate clays due to the increased surface charge, but several techniques have been developed to accomplish delamination [18]. Techniques such as stirring, sonication, or heated refluxing, are methods that tend to lead to relatively low amounts of suspended LDH colloids. Substitution of larger anionic species in between the layers, known as intercalation, is needed to facilitate the delamination process. Intercalation can be done by replacing the common chloride and nitrate ions typically present after LDH synthesis with other species such as sodium dodecylsulfate (SDS) [26,27]. After expansion of the interlayer, delamination can be achieved in organic solvents, such as formamide or various alcohols [27–29]. This is possible due to the low polarity of these solvents, and stable colloids are commonly produced from this procedure. Adachi-Pagano et al. showed that delamination of Zn-Al LDH-DS could be carried out via heated reflux in the presence of a variety of alcohols, and of those, butanol (BuOH) produced the highest LDH loadings, up to 1.5 g/L [27]. Since the incorporation of LDH into a metal matrix using electrosynthesis, to our knowledge, has not been shown previously in literature, this paper discusses the challenges of LDH incorporation into metal coatings and studies the properties, morphology, and corrosion resistance of a metal-LDH nanocomposite coating formed from an electrodeposition process.

2. Experimental

2.1. Synthesis of LDH-NO_3 powder

All reagents were analytical grade and were used as received, with no further processing. Nitrate (NO_3^-) containing layered double hydroxide was synthesized from inorganic salts by a coprecipitation method. A 600 mL solution containing 0.016 M $Zn(NO_3)_2{\cdot}6H_2O$ (Alfa Aesar) and 0.008 M $Al(NO_3)_3{\cdot}6H_2O$ (Alfa Aesar) was stirred and refluxed under nitrogen atmosphere in decarbonated DI water at constant pH 10 (adjusted with 12.5 M NaOH (Fisher)) and 95 °C for 24 h. The solution was then aged for 24 h at room temperature. The resulting solid white product was centrifuged three times while rinsing first with decarbonated water and then twice with ethanol. The centrifuged powder was then dried in an oven at 100 °C for 12 h.

2.2. Synthesis of LDH-dodecyl sulfate (LDH-DS) powder

LDH-DS powder was formed by dissolving 2.00 g of the dried LDH-NO_3 and 5.00 g of sodium dodecylsulfate (Fisher) in 600 mL of decarbonated water. The solution was stirred under nitrogen at 23 °C for 72 h. The resulting solid white product was centrifuged, then washed repeatedly first with decarbonated water and then twice with ethanol prior to drying at 100 °C for 12 h.

2.3. Preparation of colloidal delaminated LDH suspension

LDH-DS powder (0.200 g) was added to 100 mL butanol (BuOH) (Mallinckrodt), sealed under nitrogen and refluxed at 120 °C for 16 h, according to the procedure used by Adachi-Pagano [27]. During this procedure, a translucent layer and a miniscule solid layer were observed. To calculate the percent loading of delaminated LDH in the colloid, the solid was collected and weighed and it was determined that the colloidal suspension was ~1.5% LDH by weight. This colloidal suspension was stored under nitrogen atmosphere until needed.

2.4. LDH-NO_3 and LDH-DS characterization

Characterization of synthesized LDH was carried out post drying for both LDH-NO_3 and LDH-DS powders. Infrared spectroscopy of the powders was done on a Perkin Elmer Spectrum One FTIR Spectrometer scanning from 450 to 4000 cm^{-2}. Powder X-ray diffraction (pXRD) was performed on a Rigaku Ultima III X-ray diffractometer using a copper X-ray source at 40 kV and 44 mA. Samples were scanned from 0.5 to 60° 2θ, at a step size of 0.05° and a dwell time of 1.0 s. Elemental analysis was performed by atomic absorption spectroscopy (AAS) using a Perkin Elmer Analyst 300 with both Zn and Al hollow cathode lamps. Dried LDH powder was digested in a 50/50 nitric acid/perchloric acid solution, then diluted with ultrapure water (18.2 MΩ) for AAS elemental analysis. AAS results were quantified using a standard calibration curve. Particle size of both the LDH suspension and electrochemical baths was measured by dynamic light scattering (DLS) with a Beckman Delsa Nano-HC. LDH colloids were diluted to 20% v/v with ultrapure water (18.2 MΩ) and allowed to equilibrate for 60 min prior to DLS analysis.

2.5. Electrodeposition of Ni and Ni-LDH coatings

Before deposition, cyclic voltammetry (CV) for the plating baths was run using a Pine Wave Now potentiostat to determine the best plating conditions for the coatings. CVs were run at 10, 50 and 100 mV/s scan rates, starting from −0.245 V and scanning between −2.0 V and 0.5 V, respectively, then returning to −0.245 V. An EG&G PAR potentiostat/galvanostat model 273A was used for all depositions. The substrate was 430 stainless steel disks mounted in epoxy to expose only one face and polished using 400 to 1200 grit SiC paper. A final polish using a 1.0 μm alumina suspension on a felt pad was done to obtain a mirror finish. All electrodes were exposed to 5.0 M H_2SO_4 (EM Scientific) for 120 s, rinsed with DI water, and dried under nitrogen, prior to plating. Electrodeposition for both Ni and Ni-LDH films was done using a modified pulse-reverse loop consisting of −1.08 V for 10 s followed by −0.6 V for 4 s, scanning at 100 mV/s between steps, until a total charge of ~100 C (Coulombs) was reached. A saturated calomel electrode (SCE) and coiled chromel wire were used as the reference and counter electrodes, respectively. For electrodeposition of the pure nickel coatings, the electrolyte bath composition consisted of 0.10 M $NiSO_4$ (Alfa Aesar) and 0.15 M $Na_2B_4O_7$ (Fisher) adjusted to pH 3 with 5 M H_2SO_4, and addition of 5% (B1) or 10% (B2) butanol (BuOH). For the Ni-LDH nanocomposite coatings, the same electrolyte bath was used except with the addition of a 5% BuOH containing delaminated LDH colloid (BL1), or a 10% BuOH containing delaminated LDH (BL2). All solutions were adjusted to pH 3.00 ± 0.05 with 5 M H_2SO_4. All depositions were performed between 21 and 23 °C.

2.6. Ni and Ni-LDH coatings characterization

An Environmental FEI Quanta 200 scanning electron microscope (SEM) with an EDT detector coupled with an EDS energy-dispersive X-ray spectrometer was used to study the morphology of the coatings. pXRD was run for the coatings and measured from 35 to 100° 2θ on a Seimens D-500 X-ray diffractometer using a X-ray copper X-ray source set to 35 kV and 24 mA and scanned at a step size of 0.05° and 1 s dwell time.

To determine the corrosion resistant properties of the Ni and Ni-LDH coatings, open circuit potential (OCP), electrochemical impedance spectroscopy (EIS), linear polarization resistance (LPR), and potentiodynamic polarization were carried out on an EG&G PAR Parstat 4000 potentiostat. The working electrode area was 1 cm^2. A SCE and platinum mesh electrode were used as the reference and counter electrodes, respectively. OCP studies were run for 4–10 days while

immersed in 3.5% NaCl solution. EIS was performed after immersion, measured at frequencies from 1×10^5 to 2×10^{-2} Hz, with a perturbation amplitude of 10 mV. To determine polarization resistance (R_p) values, linear polarization resistance (LPR) was performed on coatings by scanning ± 20 mV from OCP at a scan rate of 0.1667 mV s^{-1}. To determine E_{corr} and i_{corr} values, potentiodynamic polarization scans were subsequently performed from ± 250 mV from OCP at a scan rate of 0.1667 mV s^{-1} and calculated using the Stern-Geary equation.

Hardness and elastic modulus experiments were performed with a Hysitron TI Premier nanoindenter, using a Berkovich indenter tip, which utilized a constant stiffness standard hardness/modulus. Samples were tested fresh after electrodeposition and drying under N_2 gas. Samples were probed 4 times, in a 2 × 2 matrix with a 10 μm spacing, to a depth of 300 nm under a constant 8000 μN applied force.

3. Design and synthesis challenges for metal-anionic clay nanocomposite coatings

Previous research by our group has shown that incorporation of montmorillonite (a cationic clay) into a metal matrix can be accomplished electrochemically [12,14,30]. Even though the montmorillonite is not electroactive, incorporation into the metal coating can be achieved through a combination of gravity, complexation with positive metal cations, and stabilization of the platelets' solubility, due to pH fluctuations in the double layer during deposition [12]. Various LDHs have been incorporated into polymer or resin matrices [31–33]. However, incorporating LDH via electrodeposition into a metal matrix presents challenges that need to be addressed for successful nanocomposite coatings to be formed. These challenges include: 1) An organic phase at relatively high concentration in the plating bath is necessary to maintain the delamination of the LDH platelets. However, using organic solutions in electrochemistry increases the resistivity of the solution which can inhibit the plating process. 2) The mass transfer method for the LDH platelets to the electrode surface is complicated, since the LDH platelets are not electroactive. A suitable technique is needed to ensure the nanoparticles reach the electrode surface during electrodeposition. 3) The pH must be suitable for both metal deposition and LDH stability to prevent flocculation or degradation of the platelets.

Addressing these challenges requires modification of the plating bath and development of a suitable electrodeposition technique. 1) *How to electrodeposit the metal nanocomposite coatings from aqueous-organic plating baths*. The selection process of suitable organic modifiers was examined in order to facilitate codeposition of LDH within the nickel matrix. The most common continuous phases for delamination of LDH are medium chain alcohols [34,35]. However, the addition of these unsaturated alcohols in too high concentrations has been shown to shut down the deposition reaction. Typically no more than 50 mmol (~0.05%) of alcohol can be added to the plating solution without deleterious effects. Scant research has been conducted with saturated monols as additives for nickel electrodeposition. Previous work by the authors studied the effect of BuOH addition in the plating bath for nickel deposition [36]. It was shown that nickel coatings could be successfully deposited from plating baths containing 5 and 10% BuOH. These concentrations are high enough to allow loading of delaminated LDH into the plating solutions without adversely affecting the nickel deposition. Butanol was selected as a prime candidate for delamination, due to its high loading capacity for LDH colloids, but had not been studied as a plating bath additive. Therefore, BuOH is a prime candidate as an additive in this study. Sodium borate was also selected as a bath additive for its exceptional complexing ability for nickel electrodeposition. Additionally, the borate is not a strong binding anion for LDH, due to its many coexisting forms in solution [37]. It can also be used in high concentrations without detrimental adsorption onto the LDH platelets, affecting complexation with nickel. This aqueous-organic bath system can help stabilize the LDH nanoplatelets in solution during nickel deposition.

2) *How to encourage incorporation of LDH nanoparticle platelets into the nickel matrix during electrodeposition*. Depositions were carried out in an inverted electrochemical cell, similar to previous work performed by our group [13,14,38]. The inverted cell design allows for better inclusion of LDH into the nickel films, where gravity and the positive charge of the platelets assists the migration of platelets to the electrode surface, with no observable flocculation during deposition. N_2 was bubbled through solution for convection and to prevent any possible flocculation of LDH on the electrode surface, which can inhibit deposition. A modified pulse reverse loop was used to help with migration problems, due to the low mobility of the nanoparticles into the double layer. The pulse loop was applied, and a scan rate chosen to allow sufficient repopulation of species near the electrode.

3) *How to prevent destabilization and/or flocculation of the LDH platelets*. A pH of 3 allows for suitable nickel deposition while not damaging the crystalline structure of LDH during deposition. All plating baths were pH adjusted with 5 M H_2SO_4 prior to the introduction of LDH and BuOH to prevent agglomeration and deterioration of the platelets. By addressing the above challenges, the authors have successfully synthesized Ni-LDH metal matrix nanocomposite coatings on steel substrate. Fig. 1 illustrates the overall process developed to produce the LDH colloid, introduce delaminated LDH platelets into the modified plating bath, and electrodeposit smooth, uniform Ni-LDH nanocomposite coatings. Details of each of these steps and the results are expanded upon in the next section.

4. Results and discussion

4.1. Characterization of LDH-NO_3 and -DS powders and colloids

Synthesis of LDH-NO_3 was carried out under nitrogen atmosphere to prevent contamination of CO_2, since the carbonate ion binds strongly to LDH and prevents delamination. A coprecipitation method was chosen because the resultant LDH precipitate has smaller particle sizes and readily delaminates, unlike more crystalline samples derived from urea hydrolysis methods [39,40]. Elemental analysis by AAS of the LDH-NO_3 precipitate indicated that for a 2:1 Zn:Al salt starting ratio, the crystalline solid formed had a ratio of 79:21 (± 1.4) wt% Zn:Al. For both the coprecipitation steps and SDS intercalation, the precipitate was isolated by repeated washing with decarbonated water and ethanol, to remove adsorbed contaminants and excess surface water. The products were dried after washing, at 100 °C for 12 h. This temperature allowed for rapid desorption of excess water and some of the interlayer water without calcining the product. This step also allowed better FT-IR and pXRD diffraction analysis for the -NO_3 and -DS intercalated LDH.

FT-IR spectroscopy results for LDH-NO_3 and LDH-DS powders are shown in Fig. 2 and consistent with literature [37]. The spectrum for (a) LDH-NO_3 has two peaks for layer and interlayer O—H stretching and bending for the metal hydroxide and water at 3568 cm^{-1} and 1621 cm^{-1}. The peaks at 1385 and 964 cm^{-1} is due to NO_3 stretching, indicating NO_3^- in the interlayer spacing. The FT-IR results for (b) LDH-DS are also consistent with literature [26]. The two C—H stretching peaks at 2854 and 2923 cm^{-1}, and S—O stretching from the sulfate head at 1207 cm^{-1} are from the dodecylsulfate structure. The 1385 cm^{-1} nitrate peak is not present in the LDH-DS sample, indicating successful intercalation of SDS and removal of nitrate ions from the interlayer of LDH.

pXRD was run on LDH-NO_3 and LDH-DS powders, and the results shown in Fig. 3. Basal spacing for (a) LDH-NO_3 is 9.06 Å, indicated by the (003) reflection, which is slightly higher than typically reported. This is due to the additional water still left after the low temperature drying process [29]. The LDH-DS powder results (Fig. 3b) show that both the (003) and (006) reflections are shifted to lower 2θ values. This shift signifies an increase in basal spacing to 37.56 Å due to intercalation of -DS in the interlayer and is consistent with literature [24]. Both

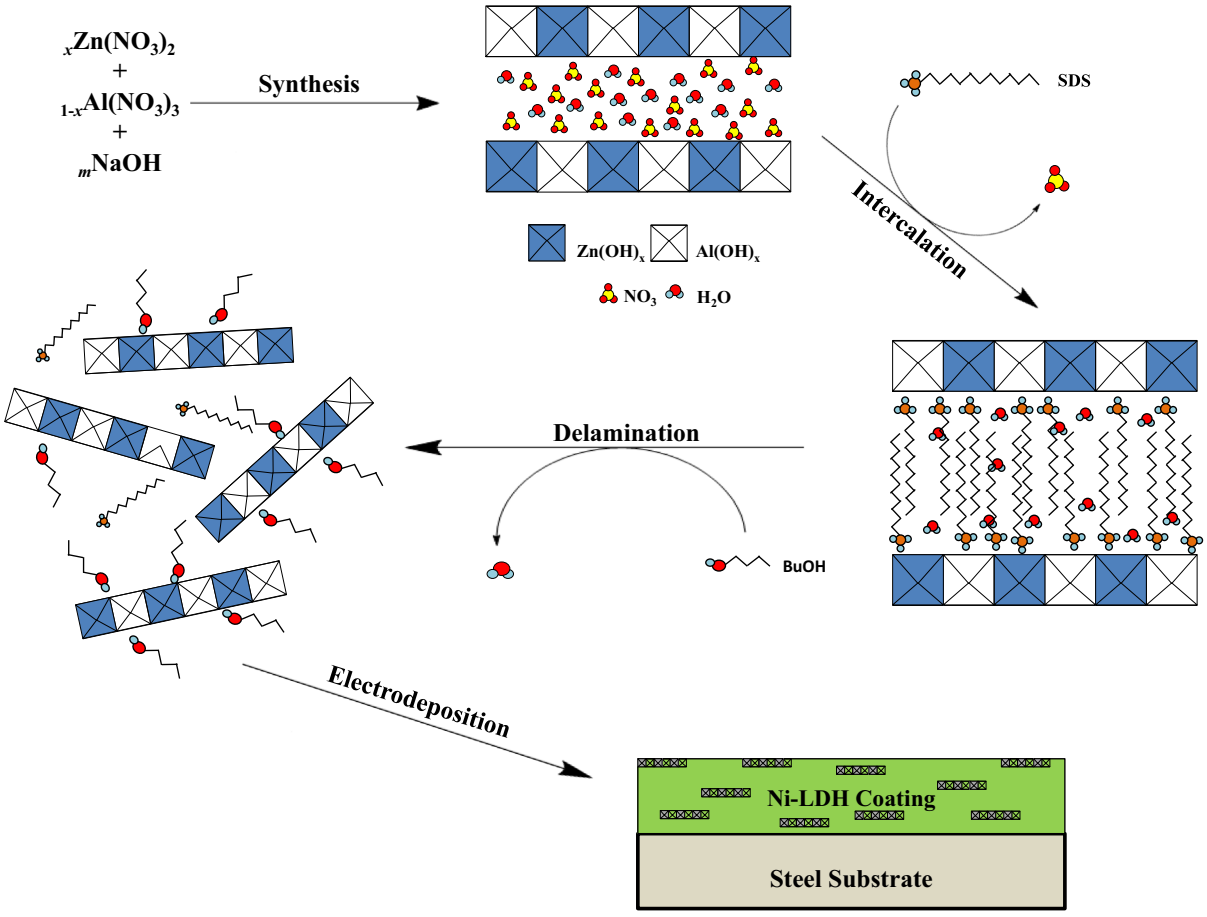

Fig. 1. Overview of the layered double hydroxide colloid synthesis and Ni-LDH metal matrix nanocomposite coating process.

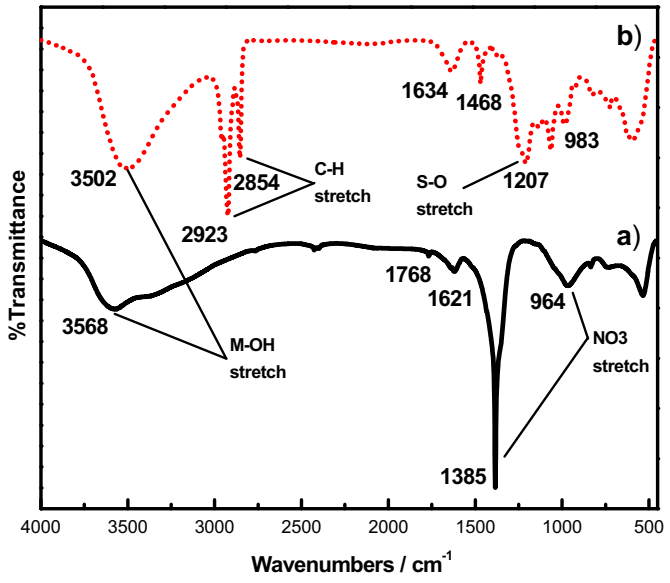

Fig. 2. FT-IR spectra of a) LDH-NO_3 (solid line), and b) LDH-DS (dotted line) powders scanned from 450 to 4000 cm^{-2}.

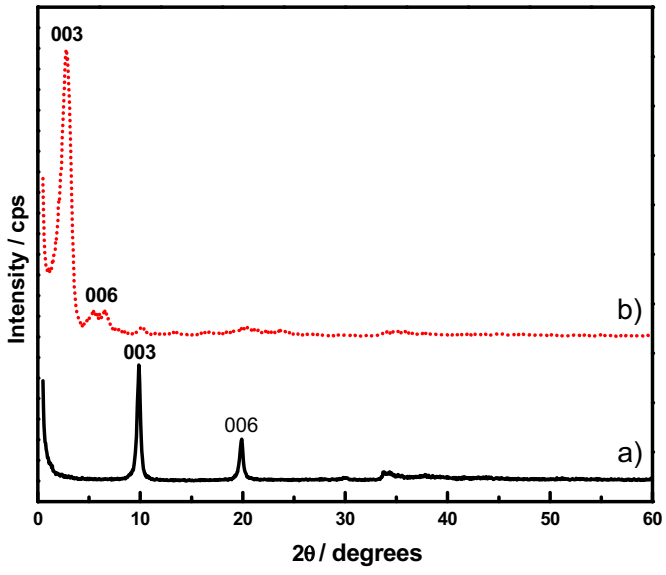

Fig. 3. Powder XRD patterns of a) LDH-NO_3 (solid line), and b) LDH-DS (dotted line) powders.

FT-IR and pXRD results show no evidence of carbonate contamination, which can inhibit intercalation and delamination of the LDH platelets.

Delamination of the LDH-DS was accomplished after refluxing, giving 1.5 ± 0.08 g of loading in the colloid. The colloid appearance changes from cloudy to translucent after delamination, signifying a change in particle size (Supplemental Fig. 1). Particle size analysis was performed on the colloid to measure the size of delaminated LDH platelets in solutions containing electrolyte salts. These particle size values are listed in Table 1. LDH solutions were measured after delamination (a) and after the delaminated solution pH was adjusted to 3.0 (b), since the electrodepositions were run at pH 3.0. The delaminated LDH particles show little size difference with a pH adjustment, and have a

Table 1
Particle size measured by DLS for (a) 20% delaminated LDH colloid in H_2O, (b) solution (a) adjusted to pH 3, (c) solution (b) + 0.1 M $NiSO_4$, (d) solution (b) + 0.15 M boric acid, (e) solution (b) + 0.1 M $NiSO_4$ + 0.15 M borate.

	$NiSO_4$ (M)	$Na_2B_4O_7$ (M)	BuOH/H_2O (%)	pH	LDH (wt %)	Particle size (nm)
a	0	0	20	8.2	0.04	631 ± 43
b	0	0	20	3.0	0.04	673 ± 198
c	0.1	0	20	3.0	0.04	620 ± 128
d	0	0.15	20	3.0	0.04	1793 ± 438
e	0.1	0.15	20	3.0	0.04	1335 ± 623

lateral dimensions of 500–800 nm. When $NiSO_4$ is added to the LDH solution (c), the particle size of LDH is unaffected by the addition of the electrolyte. However, when borate is added to the LDH suspension (d), there is a 3 fold increase in the particle size, indicating some association between the borate species in solution and the LDH particles. The addition of both nickel ions and sodium borate in the LDH solution (e) has a value in between samples (c) and (d), indicating that when both LDH nanoparticles and nickel cations are present, these both compete to adsorb or complex with borate species in solution [41].

4.2. Solution studies of Ni-LDH plating baths

The bath modifications and plating conditions were validated with CV studies to determine if addition of LDH to the plating bath affected the deposition potential for nickel or inhibited the current density. The authors showed previously that the presence of butanol causes a cathodic shift in the reduction potential of nickel by destabilizing the nickel borate complex in the double layer and by adsorbing on the electrode [36]. CVs of the plating solutions with and without LDH were run and the resulting reduction peak potentials, E_{pc}, along with current peak values, I_{pc}, Supplemental Table 1). Supplemental Fig. 2 (a–d) shows the CV scans of the plating solutions. There is no significant shift in the reduction potential for nickel when LDH nanoparticles are present in the plating solution. The reduction peak potential, E_{pc}, averages around −1.23 V for all the solutions. Also, the peak current remains in the 15–16 mA range for all the plating solutions. The inset for each graph is a Randles-Sevcik plot of current density versus square root of the scan rate. Current density increased linearly with the square root of scan rate for all plating solutions. All CVs had a crossover point near −1.08 V for all the plating baths, indicating nucleation of nickel onto the electrode during scanning. CV studies show that in the presence of the non-electroactive nanoparticle LDH platelets, there is no effect on the reduction potential of nickel for the solutions. So using a pulse deposition potential from −1.08 V for 10 s followed by −0.6 V for 4 s kept the cathodic potential away from the hydrogen evolution process and produced compact nickel and nickel nanocomposite coatings.

4.3. Characterization of electrodeposited nickel-LDH coatings

Fig. 4 shows the pXRD patterns for the electrodeposited pure Ni and Ni-LDH coatings. All the coatings have a preferred (220) orientation. Incorporation of LDH platelets into the coating does not affect the crystal orientation of the Ni-LDH nanocomposite coatings. To determine other effects of LDH inclusion, Williamson-Hall analysis was used to measure the crystallite size and particle strain for the coatings. Results are listed in Table 2 showing the coatings are nanocrystalline with crystallite size ranging from ~25 to 60 nm. Incorporation of LDH into the nickel coating causes a decrease in crystallite size, indicating that LDH nanoparticles in the coating disrupt crystalline growth. BL1 with less LDH in the film has a crystallite size of ~41 nm, while BL2 containing more LDH nanoparticles has a crystallite size of ~25 nm. For all coatings, strain was minimal, indicating relaxation during crystal growth, even during LDH inclusion. Relative texture coefficients (RTC)

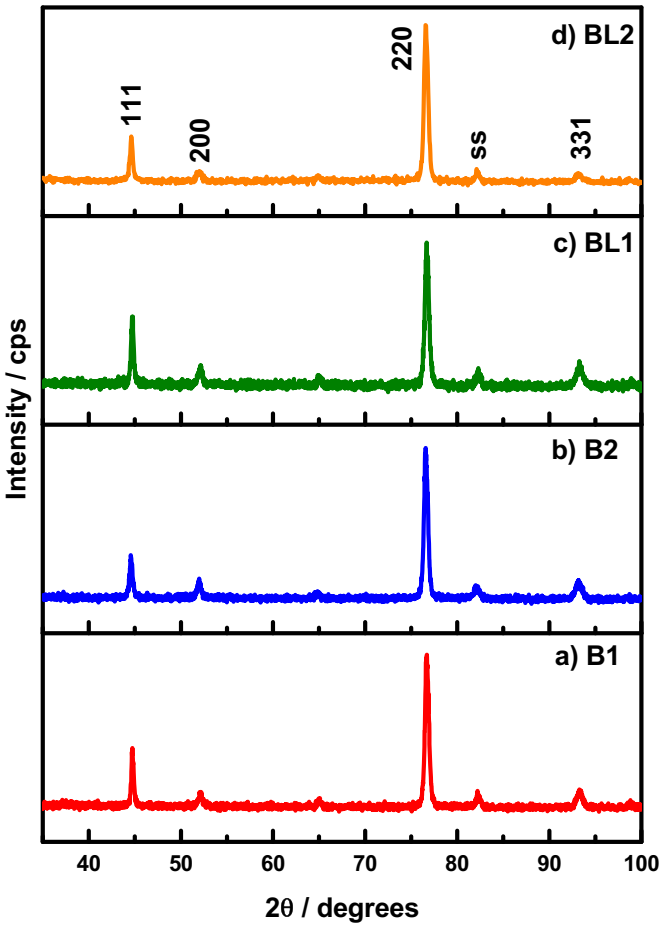

Fig. 4. Powder XRD patterns for nickel coatings a) B1, b) B2, and Ni-LDH composite coatings c) BL1, and d) BL2.

were calculated for the coatings and values are also listed in Table 2. All samples have a strong (220) character with smaller amounts of (111), (200), and (311) growth. B1 and B2 have (220) coefficients of 75.93 and 72.36, respectively, which is consistent with previous analysis of nickel coatings deposited by an electrochemical method [34]. Samples BL1 and BL2 have higher (220) character, showing that the lateral growth planes expressed by the (220) reflection are inhibited when there is LDH platelet inclusion in the nickel matrix.

SEM and EDS analysis were run to determine surface morphology and chemical composition of the coatings and results displayed in Fig. 5 and Table 3. All SEM images show dense compact crystalline films for both pure nickel and nickel nanocomposite coatings. EDS analysis determines elemental composition on the coating surfaces and can help determine if LDH is present in the coatings. The values for Ni, Al, and Zn are listed in Table 3. Aluminum was found in all coatings, since alumina is used in the polishing preparation process for the substrate surfaces. However, aluminum concentration for the pure nickel coatings, samples B1 and B2, were lower than those percentages in the nanocomposite coatings. The zinc concentration for the pure nickel samples was below the limit of detection of the experiment. The LDH containing nanocomposite samples, BL1 and BL2, had zinc concentration of 0.565% and 0.595%, respectively, indicating successful inclusion of LDH nanoparticles into the coatings.

Hardness and elastic modulus were measured via nanoindentation, with a depth profile of roughly 5% of total coating thickness. Table 4 displays the hardness and elastic modulus values for the coatings. The hardness values for all coatings are in the range of 6–7 GPa, with BL1 displaying slightly better hardness. These hardness values are in the same range as for nanocrystalline nickel coatings. Li et al. showed that

Table 2
Crystallite size and strain measured from Williamson-Hall analysis and results of relative texture coefficient analysis of the XRD patterns of Ni and Ni-LDH coatings.

	Crystallite size (nm)	Strain	RTC_{111}	RTC_{200}	RTC_{220}	RTC_{311}
B1	37.54 ± 27	0.0228 ± 0.013	10.04 ± 5.5	5.84 ± 2.2	75.93 ± 9.0	8.19 ± 1.5
B2	60.20 ± 21	0.0192 ± 0.001	9.86 ± 6.0	8.66 ± 4.6	72.36 ± 12.0	9.12 ± 2.0
BL1	41.16 ± 2	0.0120 ± 0.007	6.25 ± 0.2	3.40 ± 1.0	84.94 ± 4.5	5.41 ± 3.3
BL2	25.10 ± 6	0.0158 ± 0.017	8.22 ± 1.8	5.88 ± 3.3	78.91 ± 8.6	6.99 ± 3.7

monolayer LDH displays remarkable flexibility [42], which suggests that unlike other ceramic additives to Ni composite coatings, LDH would not lead to a large increase in hardness for the composite. This small effect in hardness for the composite coatings has been observed in untreated nickel-carbon nanotube composites as well [43,44]. Elastic modulus values also show little change when LDH is dispersed into the nickel matrix and range from ~195 to 240 GPa.

4.4. Corrosion resistance of Ni-LDH coatings

After deposition, all samples were rinsed thoroughly with DI water, dried with N_2 gas, and immersed in 3.5% NaCl solution to monitor the oxidation and corrosion process. The open circuit potential (OCP) for the coatings was initially monitored for a period of 14 days to assess the degree of corrosion for all samples (Supplemental Fig. 3). After 14 days, the pure nickel coatings, B1 and B2, have OCP values cathodic to the nanocomposite coatings and small visible signs of Fe_2O_3 corrosion products on the coating surface, indicating attack by the salt solution causing coating failure. For the nanocomposite coatings, BL1 and BL2, OCP stabilizes near −0.35 V, indicating a slow oxide film growth and no visible presence of Fe_2O_3. To study the growth of the nickel oxide layer for both Ni and Ni-LDH coatings, 4 days immersion was selected for samples B1 and B2, and 10 days for BL1 and BL2. These times were selected since they are prior to coating failure at 14 days noted by the appearance of corrosion products on the coating surface. Samples BL1 and BL2 were also tested at 4 days immersion to show the slower oxide

Table 3
EDS elemental analysis results for Ni, Al, and Zn of the electrodeposited coatings.

	% Ni	% Al	% Zn
B1	99.66	0.338	–
B2	99.63	0.370	–
BL1	98.97	0.468	0.565
BL2	98.83	0.575	0.595

Table 4
Hardness and elastic modulus values for Ni (B1, B2) and Ni-LDH (BL1, BL2) coatings.

	Hardness (GPa)	Elastic modulus (GPa)
B1	6.11 ± 0.07	239.90 ± 5.84
B2	6.43 ± 0.37	200.28 ± 11.92
BL1	6.90 ± 0.18	194.73 ± 4.46
BL2	6.07 ± 0.15	205.16 ± 10.01

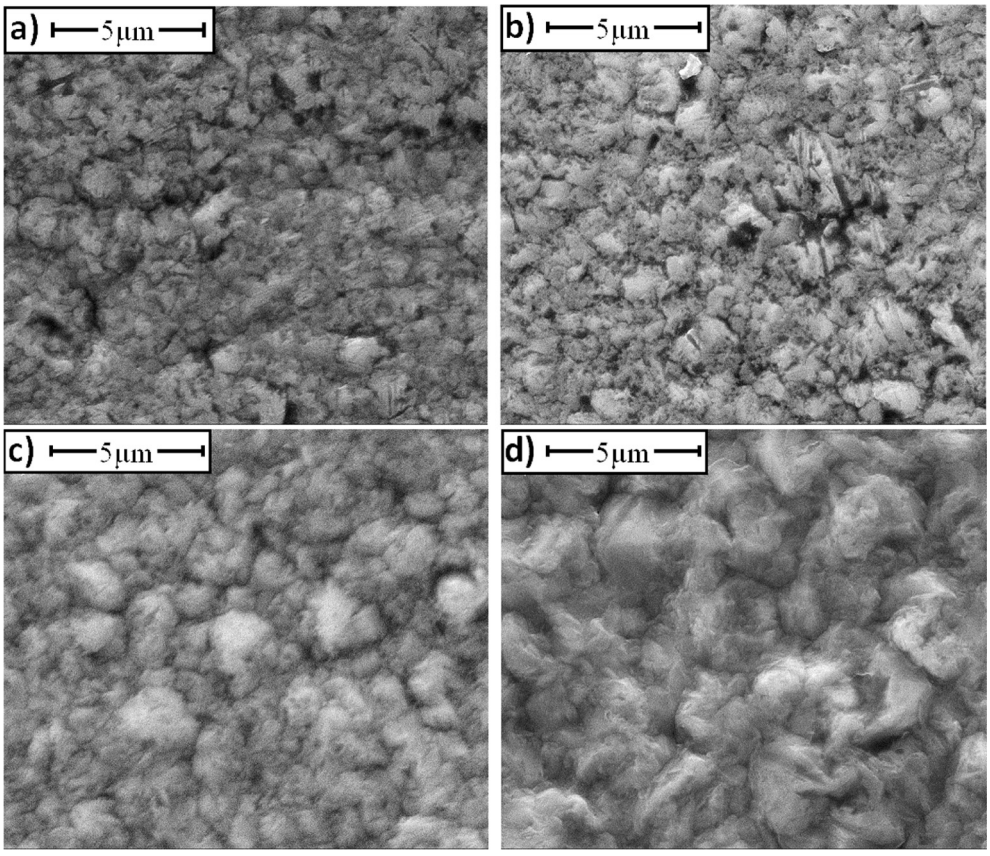

Fig. 5. SEM images of each nickel coating a) B1, b) B2, and Ni-LDH composite coatings, c) BL1, and d) BL2. Scale bars are 5 μm.

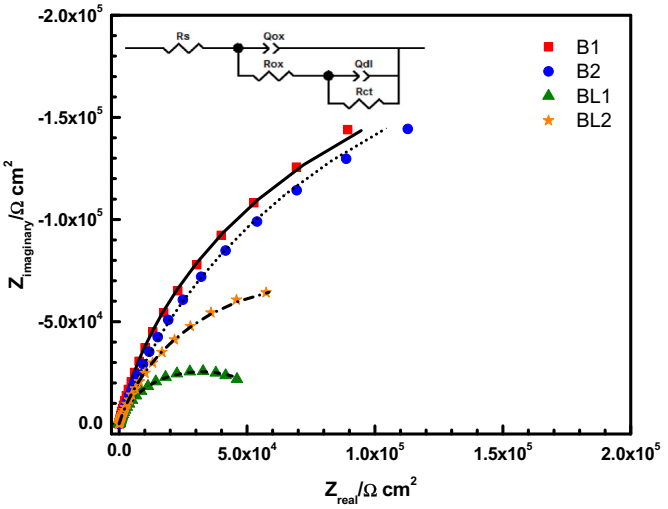

Fig. 6. Nyquist plots and theoretical fittings for nickel coatings, B1, B2, and Ni-LDH composite coatings, BL1, BL2, after 4 days immersion in 3.5% NaCl. The inset circuit was used for fitting. Black lines are the Zview fitting curves and symbols represent experimental data.

formation due to LDH inclusion. The LDH inclusion did successfully slow down the formation of an oxide film and additional corrosion tests were run to study this effect.

4.4.1. Electrochemical impedance spectroscopy

EIS was performed on each sample after immersion in a 3.5% NaCl solution for times discussed in the previous section. Once a stable OCP was reached, typically after 1 h immersion in fresh 3.5% NaCl solution, the stainless steel substrates with coatings were measured with EIS. Nyquist plots for the samples are shown in Figs. 6 and 7 and display a semicircle loop. Figs. 8 and 9 are the magnitude and phase angle plots for the samples. ZView software was used to design the equivalent circuit and analyze the EIS data fittings to predict the corrosion behavior of the coatings based off of a circuit model.

Based on the OCP studies, and SEM results, a circuit was chosen that describes a porous oxide layer present at the surface interface, with an intact nickel or Ni-LDH layer underneath. The most accurate fit corresponds to this equivalent circuit shown in the inset of Fig. 6. The selected circuit has a solution resistance, a constant phase element and

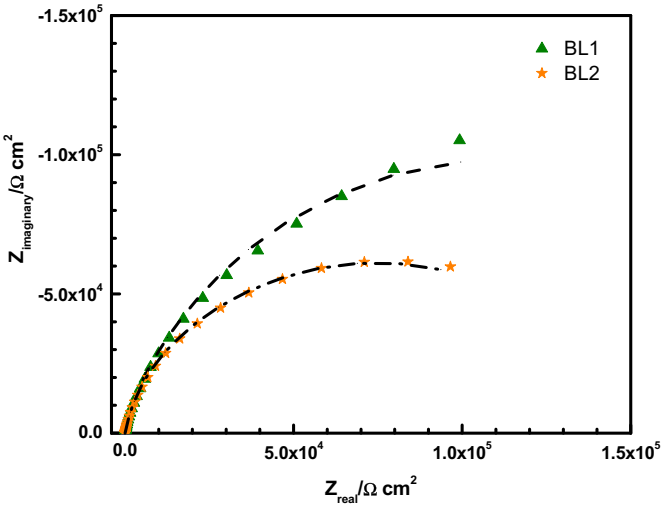

Fig. 7. Nyquist plots and fittings for Ni-LDH composite coatings BL1, BL2 after 10 days immersion in 3.5% NaCl Circuit used for fitting inset in Fig. 6. Black lines are the Zview fitting curves and symbols represent experimental data.

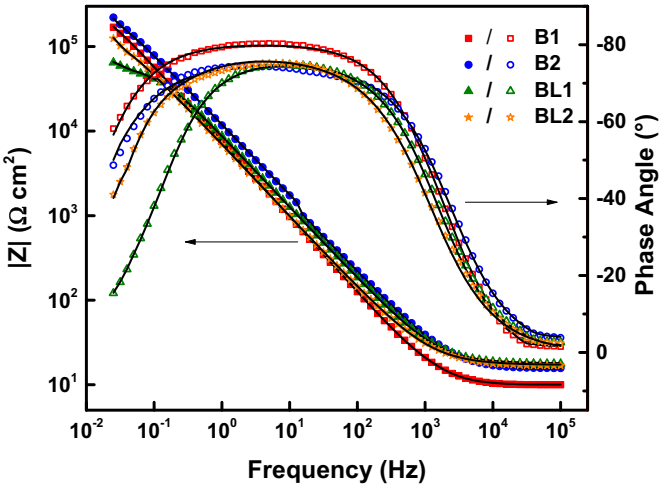

Fig. 8. Bode plots for magnitude and phase angle with fittings for nickel coatings, B1, B2, and Ni-LDH composite coatings, BL1, BL2, after 4 days immersion in 3.5% NaCl. Black lines are the Zview fitting curves and symbols represent experimental data.

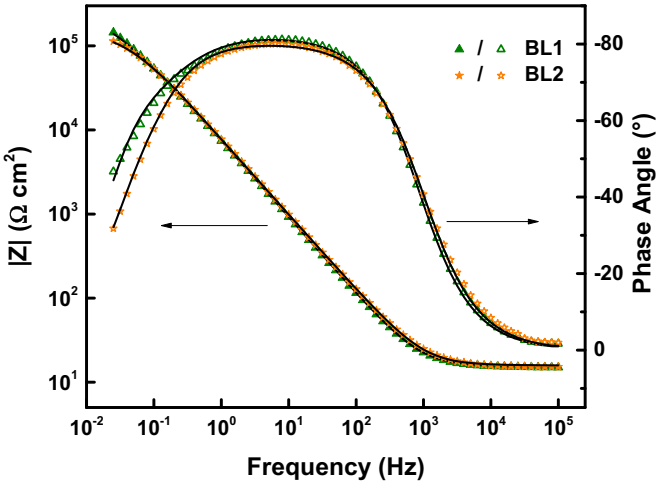

Fig. 9. Bode plots for magnitude and phase angle with fittings for Ni-LDH composite coatings BL1, BL2 after 10 days immersion in 3.5% NaCl. Black lines are the Zview fitting curves and symbols represent experimental data.

resistance for the porous oxide layer, and a constant phase element and resistance for the interface at the surface of the nickel or Ni-LDH coatings. The selected circuit model consisted of three resistors and two constant phase elements (inset Fig. 6). Resistors include a value for the solution resistance (R_s), the resistance of the nickel oxide layer (R_{ox}), and the charge transfer resistance of the coating (R_{ct}). Each constant phase element has two values: Q, an equivalent capacitance calculated from the parameters found from fitting the data with the selected circuit diagram, and a coefficient α, which represents a measure of similarity to a capacitor, ranging from 0 to 1 with 1 being identical to a capacitor. Q_{ox} represents the behavior of the oxide layer formed after immersion, and is associated with α_1. It does not behave as a true capacitor since it is a porous oxide layer. Q_{dl} and the associated α_2, represent the behavior of the double layer capacitance arising from the double layer formed at the interface of the solution and the nickel coating at the bottom of the pores in the oxide layer.

The solution resistance, R_s value is affected by the distance between the counter electrode and coating samples in solution and is between 14.5 and 17.1 Ω cm^2, shown in Table 5, for all samples, which are typical values for these salt solutions. The pure nickel samples, B1 and B2 have larger R_{ox} values, at 331.8 and 229.4 kΩ cm^2, which indicates a

Table 5
Electrochemical impedance spectroscopy data for B1 and B2 after 4 days, and BL1 and BL2 after 10 days immersion in 3.5% NaCl solution.

	Immersion (days)	R_s (Ω cm^2)	Q_{ox} (uF cm^{-2})	α_1	R_{ox} (kΩ cm^2)	Q_{dl} (uF cm^{-2})	α_2	R_{ct} (kΩ cm^2)
B1	4	14.5 ± 2.8	7.9 ± 0.3	0.895	331.8 ± 68.7	1.6 ± 0.7	0.741	1.4 ± 0.2
B2	4	17.1 ± 0.9	7.2 ± 1.9	0.861	229.4 ± 20.8	4.5 ± 0.3	0.820	1.7 ± 0.5
BL1	4	15.2 ± 1.5	5.3 ± 0.4	0.865	10.4 ± 5.5	5.5 ± 0.9	0.670	93.4 ± 15.2
	10	15.9 ± 2.1	10.0 ± 0.5	0.788	119.2 ± 13.2	17.2 ± 1.5	0.899	138.9 ± 67.9
BL2	4	16.5 ± 1.1	2.8 ± 0.8	0.812	7.8 ± 3.4	2.4 ± 0.3	0.704	323.1 ± 81.2
	10	15.1 ± 1.7	12.8 ± 3.5	0.849	115.7 ± 22.3	22.0 ± 1.1	0.931	102.7 ± 23.4

well formed oxide layer. The Ni-LDH coating samples have lower R_{ox} values than B1 or B2 at only 4 days of immersion time, as indicated by the much smaller semicircle patterns in the Nyquist plots. Comparing the Nyquist plots of BL1 and BL2 after 10 days immersion however, it is evident that oxide layer formation was still occurring between days 4 and 10, as shown in Fig. 7, but R_{ox} values for the nanocomposite coatings are still lower than pure nickel coatings, with values of 119.2 and 115.7 kΩ cm^2, respectively. The lower R_{ox} values suggest that the inclusion of LDH into the nickel coating does slow the rate of nickel oxide formation and hinders the formation of the passive oxide layer. It can be seen from the Bode plots in Fig. 8 that after 4 days the pure Ni coatings, B1 and B2, have formed a more complete oxide layer compared to the Ni-LDH samples, BL1 and BL2, as evidenced by the higher phase angles over a large frequency range. However, when the oxide layer is allowed to progress for the Ni-LDH samples (BL1 and BL2) from 4 to 10 days, a more complete oxide layer is formed as indicated by a higher phase angle values when comparing Figs. 8 and 9 for Ni-LDH. This slower rate of oxide growth is even more evident if you compare the ZView values for the BL1 and BL2 coatings for 4 days and 10 days. The oxide layer formed after 10 days may be thinner than that of their B1 and B2 counterparts, or oxide formation may be incomplete in areas of LDH presence at the surface of the coatings. However, the oxide layer capacitance, Q_{ox}, of BL1 and BL2 has higher values at 10.0 and 12.8 μF cm^{-2} after 10 days, which shows that if there are any gaps present in the oxide layer, the presence of LDH has an effect at the interface. This effect could not be explicitly discerned from the spectra, so it was not included as part of the circuit. Additionally, comparison between 4 and 10 days for BL1 and BL2 show a consistent increase in capacitance. The increase in capacitance would also have a slowing effect on the formation of the nickel oxide layer. The R_{ct} values for B1 and B2 coatings are much lower than the nanocomposite coatings for either Ni-LDH measurement time. This indicates that the inclusion of LDH nanoplatelets leads to higher R_{ct} values for the nanocomposite coatings and an improvement in corrosion resistance, even though the oxide layer formation for the composite coatings may be slower. The Ni-LDH coating may have a lower active area available for the corrosion attack when compared to the nickel coatings. Similar results have been seen for other electrochemically deposited nickel nanocomposite coatings, which also used the same circuit diagram. In those studies the R_{ct} value increased and corrosion resistance improved with the addition of ceramic nanoparticles such as Al_2O_3 or SiC into the nickel coating compared to the nickel only coating [45–47].

4.4.2. Potentiodynamic polarization

Each sample was analyzed using LPR and potentiodynamic polarization. From LPR, the polarization resistance, R_p, was calculated to determine the overall corrosion resistance of the films. Corrosion potential, E_{corr}, and the anodic (β_a) and cathodic (β_c) slopes were measured from the potentiodynamic scans, shown in Fig. 10. The corrosion current, i_{corr}, was then determined from the Stern-Geary equation. Results of the LPR and potentiodynamic polarization measurements are listed in Table 6. For all coatings, E_{corr} values are similar, with E_{corr} of BL1 shifted ~60 mV anodic to the other samples. R_p for all samples is above 200 kΩ cm^2 showing good corrosion resistance. B1 displays the largest R_p value indicating the coating has a well formed oxide layer,

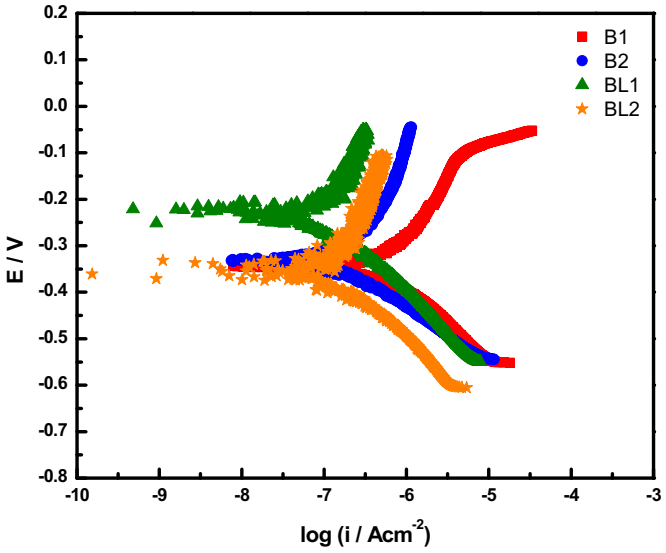

Fig. 10. Linear polarization curves for nickel coatings, B1, B2, and Ni-LDH composite coatings, BL1, BL2, coatings after 4 days immersion in 3.5% NaCl.

consistent with EIS results. LDH containing samples display a trend that indicates LDH inclusion does improve corrosion resistance. Though BL1 displays a relatively low R_p, at 232.3 kΩ cm^2, BL2, with higher percentage of LDH in the coating, has the second largest R_p values at 342.5 kΩ cm^2. This difference suggests that increased LDH percentage in the coating does improve corrosion resistance but the inclusion of LDH slows down the formation of the passive oxide layer. Any LDH at the surface is likely to create breaks or holes in the passive oxide layer, since nickel oxide would not readily form over the top of the platelets.

The anodic slope of the potentiodynamic polarization curve, β_a shows this in more detail. B1 displays a lower anodic slope value than B2 by 100 mV dec^{-1}. This same trend is true for BL1 and BL2. Both BL1 and BL2 have an observed slope increase of 100 mV dec^{-1} compared to the control nickel samples, due to the inclusion of LDH. This shows that addition of LDH nanoparticles does help improve coating corrosion resistance, and the difference between the BL1 and BL2 slopes is the same as that of B1 and B2, consistent with the increase in BuOH addition in the plating bath. The i_{corr} values for the Ni and Ni-LDH coatings are all within the same range giving a relatively slow corrosion rate. With Zn as the divalent metal in the LDH coatings, there may be some small amount of sacrificial corrosion occurring.

The scope of this work was to determine if delaminated LDH platelets could be incorporated into a metal matrix to increase the corrosion resistance over pure metal films. The choice of other divalent and trivalent metals in the LDH structure may have a profound effect on the corrosion resistance of the nanocomposite coatings. Specifically, studying Mg/Al, Ni/Al, Ni/Cr, and Zn/Cr varieties could be of interest. Mg/Al is one the most commonly found LDH species, and is expected to perform well as a corrosion inhibitor due to the inertness and stability of the species involved. LDH structures that contain metals commonly used as anti-corrosion coatings, such as Ni/Al, Ni/Cr, and Zn/Cr would

Table 6
Potentiodynamic polarization data for B1 and B2 after 4 days, and BL1 and BL2 after 10 days immersion in 3.5% NaCl.

	E_{corr} (V vs. SCE)	i_{corr} (μA cm^2)	β_c (V dec^{-1})	β_a (V dec^{-1})	R_p (kΩ cm^2)
B1	−0.330 ± 0.03	0.363	−0.167 ± 0.01	0.323 ± 0.13	412.5 ± 18.4
B2	−0.323 ± 0.02	0.465	−0.158 ± 0.03	0.433 ± 0.18	232.4 ± 22.8
BL1	−0.273 ± 0.06	0.469	−0.158 ± 0.03	0.427 ± 0.23	232.3 ± 10.3
BL2	−0.315 ± 0.04	0.391	−0.200 ± 0.05	0.567 ± 0.16	342.5 ± 27.7

be of interest to study due to their stability and oxide formation when exposed to corrosive environments. A panel study of multiple LDH elemental compositions at various M(II)/M(III) ratios and platelet sizes would allow for better optimization of the plating process and for fine-tuning of the corrosion resistance.

5. Conclusions

This work describes the addition of an anionic clay (LDH) into a nickel matrix to produce a nanocomposite coating using electrochemical deposition. The obstacles that make the production of these coatings difficult are explained and solutions are outlined. Layered double hydroxide platelets are synthesized by a coprecipitation method. The intercalation of sodium dodecyl sulfate into the LDH layers helps in delamination of the platelets to give a 1.5 g/L loading in BuOH. Dispersion of the LDH platelets into an aqueous plating solution has no effect on the deposition potential of nickel but does affect the grain size of the coatings. Powder XRD and Williamson-Hall analysis shows incorporation of the nanoplatelets into the coatings lowers the crystallite size, which is beneficial for corrosion resistance. EDS results indicate the presence of the LDH nanoplatelets in the nickel coatings. The addition of LDH in the coating slows the growth rate of the passive oxide layer based on long term immersion and EIS testing. The LDH platelets in the coatings slow the initial oxidation process of the nickel at the surface-solution interface and decrease the active surface area available for nickel oxidation. Ni-LDH composite coatings display a larger coating charge transfer resistance, which suggests Ni-LDH will perform better than pure nickel coatings in an aggressive chloride media. Further studies are needed to understand the mechanism for corrosion resistance and coating growth. Given the wide scope of future work for this new class of coatings, it could be possible to tune different combinations of LDH structures and metal matrices for specific environmental concerns. All of which may be created using a low cost, room temperature, electrodeposition process that is scalable and flexible.

Acknowledgments

This work was partially supported by the Advanced Materials and Manufacturing Processes Institute (AMMPI) at University of North Texas.

Appendix A. Supplementary data

Supplementary data to this article can be found online at https://doi.org/10.1016/j.surfcoat.2018.05.026.

References

[1] T. Lampke, A. Leopold, D. Dietrich, G. Alisch, B. Wielage, Correlation between structure and corrosion behaviour of nickel dispersion coatings containing ceramic particles of different sizes, Surf. Coat. Technol. 201 (2006) 3510–3517.
[2] E. Brooman, Compliant electrodeposited and electroless nano-structured and nano-composite coatings to replace chromium coatings part 1, Galvanotechnik 96 (12) (2005) 2843–2853.
[3] T. Lampke, B. Wielage, D. Dietrich, A. Leopold, Details of crystalline growth in co-deposited electroplated nickel films with hard (nano)particles, Appl. Surf. Sci. 253 (2006) 2399–2408.
[4] I. Garcia, A. Conde, G. Langelaan, J. Fransaer, J.P. Celis, Improved corrosion resistance through microstructural modifications induced by codepositing SiC-particles with electrolytic nickel, Corros. Sci. 45 (2003) 1173–1189.
[5] V. Torabinejad, M. Aliofkhazraei, S. Assareh, M.H. Allahyarzadeh, A.S. Rouhaghdam, Electrodeposition of Ni-Fe alloys, composites, and nano coatings - a review, J. Alloys Compd. 691 (2017) 841–859.
[6] Y. He, S.C. Wang, F.C. Walsh, Y. Chiu, P.A.S. Reed, Self-lubricating Ni-P-MoS_2 composite coatings, Surf. Coat. Technol. 307 (2016) 926–934.
[7] D.B. Miracle, Metal matrix composites – from science to technological significance, Composites 65 (2005) 2526–2540.
[8] B. Szczygiet, M. Kolodziej, Corrosion resistance of Ni/Al_2O_3 coatings in NaCl solution, Trans. Inst. Met. Finish. 83 (4) (2005) 181–187.
[9] D. Thiemig, A. Bund, Characterization of electrodeposited Ni-TiO_2 nanocomposite coatings, Surf. Coat. Technol. 202 (2008) 2976–2984.
[10] H. Zhang, Y. Zou, Z. Zou, C. Shi, Effects of CeO_2 on microstructure and corrosion resistance of TiC-VC reinforced Fe-based laser cladding layers, J. Rare Earths 32 (11) (2014) 1095–1100.
[11] M.L. Lepule, B.A. Obadele, A. Andrews, P.A. Olubambi, Corrosion and wear behaviour of ZrO_2 modified NiTi coatings on AISI 316 stainless steel, Surf. Coat. Technol. 261 (2015) 21–27.
[12] J. Tientong, Y.H. Ahmad, M. Nar, N. D'Souza, A.M.A. Mohamed, T.D. Golden, Improved mechanical and corrosion properties of nickel composite coatings by incorporation of layered silicates, Mater. Chem. Phys. 145 (2014) 44–50.
[13] Y.H. Ahmad, J. Tientong, M. Nar, N. D'Souza, A.M.A. Mohamed, T.D. Golden, Characterization and corrosion resistance of electrodeposited Ni-Mo-silicate platelet nanocomposite coatings, Surf. Coat. Technol. 259 (2014) 517–525.
[14] C.R. Thurber, M. Calhoun, Y.H. Ahmad, N. D'Souza, A.M.A. Mohamed, T.D. Golden, Electrodeposition of Cu-Ni incorporated with layered silicates for corrosion protection, ECS Trans. 61 (20) (2014) 49–60.
[15] C. Forano, U. Costantino, V. Prevot, C.T. Gueho, Layered Double Hydroxides, vol. 5A, Elsevier Ltd., 2006.
[16] T. Chen, S. Xu, F. Zhang, D.G. Evans, X. Duan, Formation of photo- and thermostable layered double hydroxide films with photo-responsive wettability by intercalation of functionalized azobenzenes, Chem. Eng. Sci. 64 (2009) 4350–4357.
[17] F. Leroux, J. Besse, Polymer interleaved layered double hydroxide: a new emerging class of nanocomposites, Chem. Mater. 13 (2001) 3507–3515.
[18] Q. Wang, D. O'Hare, Recent advances in the synthesis and application of layered double hydroxide (LDH) nanosheets, Chem. Rev. 112 (2012) 4124–4155.
[19] J. Tedim, A.C. Bastos, S. Kallip, M.L. Zheludkevich, M.G.S. Ferreira, Corrosion protection of AA2024-T3 by LDH conversion films. Analysis of SVET results, Electrochim. Acta 210 (2016) 215–224.
[20] J. Tedim, M.L. Zheludkevich, A.C. Bastos, A.N. Salak, A.D. Lisenkov, M.G.S. Ferreira, Influence of preparation conditions of layered double hydroxide conversion films on corrosion protection, Electrochim. Acta 117 (2014) 164–171.
[21] M.R. Zamanzad-Ghavidel, K. Raeissi, A. Saatchi, The effect of surface morphology on pitting corrosion resistance of Ni nanocrystalline coatings, Mater. Lett. 63 (2009) 1807–1809.
[22] B.K.A. Kumar, M.G. Ananthaprasad, K.G.A. Krishna, Review on corrosion behavior of nickel matrix composites, Int. J. Emerg. Technol. Adv. Eng. 5 (10) (2015) 342–346.
[23] N.O. San, H. Nazir, G. Dönmez, Microbially influenced corrosion and inhibition of nickel-zinc and nickel-copper coatings by *Pseudomonas aeruginosa*, Corros. Sci. 79 (2014) 177–183.
[24] T. Hibino, M. Kobayashi, Delamination of layered double hydroxides containing in water, J. Mater. Chem. 15 (2004) 653–656.
[25] B. Schneiderová, J. Demel, J. Pleštil, H. Tarábková, J. Bohuslav, K. Lang, Electrochemical performance of cobalt hydroxide nanosheets formed by the delamination of layered cobalt hydroxide in water, Dalton Trans. 43 (2014) 10484–10491.
[26] B.R. Venugopal, C. Shivakumara, M. Rajamathi, Effect of various factors influencing the delamination behavior of surfactant intercalated layered double hydroxides, J. Colloid Interface Sci. 294 (2006) 234–239.
[27] M. Adachi-Pagano, C. Forano, J.-P. Besse, Delamination of layered double hydroxides by use of surfactants, Chem. Commun. (2000) 91–92.
[28] L. Li, R. Ma, Y. Ebina, N. Iyi, T. Sasaki, Positively charged nanosheets derived via total delamination of layered double hydroxides, Chem. Mater. 17 (2005) 4386–4391.
[29] F. Leroux, M. Adachi-Pagano, M. Intissar, S. Chauvière, C. Forano, J.-P. Besse, Delamination and restacking of layered double hydroxides, J. Mater. Chem. 11 (2001) 105–112.
[30] Y.H. Ahmad, J. Tientong, N.D. Souza, T.D. Golden, A.M.A. Mohamed, Salt water corrosion resistance of electrodeposited Ni-layered silicate nanocomposite coatings from Watts' type solution, Surf. Coat. Technol. 242 (2014) 170–176.
[31] F. Leroux, Organo-modified anionic clays into polymer compared to smectite-type nanofiller: Potential applications of the nanocomposites, J. Nanosci. Nanotech. 6 (2006) 303–315.

[32] E. Kafunkova, K. Lang, P. Kubat, M. Klementova, J. Mosinger, M. Slouf, A.-L. Troutier-Thuilliez, F. Leroux, V. Verney, C. Taviot-Gueho, Porphyrin-layered double hydroxide/polymer composites as novel ecological photoactive surfaces, J. Mater. Chem. 20 (2010) 9423–9432.
[33] S. Mallakpour, M. Hatami, Condensation polymer/layered double hydroxide NCs: preparation, characterization, and utilizations, Eur. Polym. J. 90 (2017) 273–300.
[34] J. Macheras, D. Vouros, C. Kollia, N. Spyrellis, Nickel electrocrystallization: influence of unsaturated organic additives on the mechanism of oriented crystal growth, Trans. IMF 74 (2) (1996) 55–58.
[35] U. Belkis, S. Esma, K. Ramazan, The investigation of electrochemical effect of diol compounds in nickel electroplating bath, J. Mater. Sci. Eng. Adv. Technol. 8 (2) (2013) 55–68.
[36] R.E. Daugherty, M.M. Zumbach, T.D. Golden, The influence of an aqueous-butanol plating bath on the microstructure and corrosion resistance of electrodeposited nickel coatings, J. Appl. Electrochem. 47 (2017) 467–477.
[37] A. Nedim, B. Zümreoglu-karan, A. Temel, L. Mafra, Layered double hydroxides with interlayer borate anions: a critical evaluation of synthesis methodology and pH-independent orientations in nano-galleries, Appl. Clay Sci. 51 (2011) 308–316.
[38] J. Tientong, C.R. Thurber, N. D'Souza, A. Mohamed, T.D. Golden, Influence of bath composition at acidic pH on electrodeposition of nickel-layered silicate nanocomposites for corrosion protection, Int. J. Electrochem. 2013 (2013) 1–8.
[39] K. Xu, G. Chen, J. Shen, Exfoliation and dispersion of micrometer-sized LDH particles in poly(ethylene terephthalate) and their nanocomposite thermal stability, Appl. Clay Sci. 75–76 (2013) 114–119.
[40] J. Liu, J. Song, H. Xiao, L. Zhang, Y. Qin, D. Liu, W. Hou, N. Du, Synthesis and thermal properties of ZnAl layered double hydroxide by urea hydrolysis, Powder Technol. 253 (2014) 41–45.
[41] H.A. Conrad, M.R. McGuire, T. Zhou, M.I. Coskun, T.D. Golden, Improved corrosion resistant properties of electrochemically deposited zinc-nickel alloys utilizing a borate electrolytic alkaline solution, Surf. Coat. Technol. 272 (2015) 50–57.
[42] B. Li, J. He, D.G. Evans, Experimental investigation of sheet flexibility of layered double hydroxides: one-pot morphosynthesis of inorganic intercalates, Chem. Eng. J. 144 (2008) 124–137.
[43] C.R. Carpenter, P.H. Shipway, Y. Zhu, The influence of CNT co-deposition on electrodeposit grain size and hardness, Surf. Coat. Technol. 205 (2011) 5059–5063.
[44] S. Khabazian, S. Sanjabi, The effect of multi-walled carbon nanotube pretreatments on the electrodeposition of Ni – MWCNTs coatings, Appl. Surf. Sci. 257 (2011) 5850–5856.
[45] B. Szczygieł, M. Kołodziej, Composite Ni/Al_2O_3 coatings and their corrosion resistance, Electrochim. Acta 50 (2005) 4188–4195.
[46] S. Özkan, G. Hapçı, G. Orhan, K. Kazmanlı, Electrodeposited Ni/SiC nanocomposite coatings and evaluation of wear and corrosion properties, Surf. Coat. Technol. 232 (2013) 734–741.
[47] Y. Zhou, F.Q. Xie, X.Q. Wu, W.D. Zhao, X. Chen, A novel plating apparatus for electrodeposition of Ni-SiC composite coatings using circulating-solution co-deposition technique, J. Alloys Compd. 699 (2017) 366–377.